CrystEngComm

# Photosensitized samarium(III) and erbium(III) complexes of planar N,N-donor heterocyclic bases: crystal structures and evaluation of biological activity



| | |
|---|---|
| Journal: | *CrystEngComm* |
| Manuscript ID | CE-ART-12-2015-002387.R1 |
| Article Type: | Paper |
| Date Submitted by the Author: | 22-Jan-2016 |
| Complete List of Authors: | Dasari, Srikanth; INDIAN INSTITUTE OF TECHNOLOGY KANPUR, DEPARTMENT OF CHEMISTRY<br>Abbas, Zaffar; Indian Institute of Technology Kanpur, Chemistry<br>Kumar, Priyaranjan; Indian Institute of Technology Kanpur, Chemistry<br>Patra, Ashis; Indian Institute of Technology Kanpur, Chemistry |
| | |

Journal Name

ARTICLE

# Photosensitized samarium(III) and erbium(III) complexes of planar *N,N*-donor heterocyclic bases: crystal structures and evaluation of biological activity†

Received 00th January 20xx,
Accepted 00th January 20xx

DOI: 10.1039/x0xx00000x

www.rsc.org/

Srikanth Dasari, Zafar Abbas, Priyaranjan Kumar and Ashis K. Patra*

The samarium(III) and erbium(III) complexes, namely $[Sm(dpq)(DMF)_2(H_2O)Cl_3]$ (**1**), $[Sm(dppz)(DMF)_2(H_2O)Cl_3]$ (**2**), $[Er(dpq)(DMF)_2Cl_3]$ (**3**), and $[Er(dppz)_2Cl_3]$ (**4**), where dipyrido[3,2-*d*:2′,3′-*f*]quinoxaline (dpq in **1** and **3**), dipyrido[3,2-*a*:2′,3′-*c*]phenazine (dppz in **2** and **4**) and *N*,*N*′-dimethylformamide (DMF) water ($H_2O$) have been synthesized and structurally characterized. The X-ray crystal structures of complexes **1**-**4** showing discrete mononuclear Ln(III)-based structures. The Sm(III) in $[Sm(dpq)(DMF)_2(H_2O)Cl_3]$ (**1**) and $[Sm(dppz)(DMF)_2(H_2O)Cl_3]$ (**2**), as adopts a eight-coordinated distorted square antiprism structure with a bidentate *N*,*N*-donor dpq/dppz ligand, three $Cl^-$ anions, two DMF and one water molecule. The Er(III) complexes, $[Er(dpq)(DMF)_2Cl_3]$ (**3**), and $[Er(dppz)_2Cl_3]$ (**4**) show a seven-coordinated mono-capped octahedron structure where Er(III) coordinated to a bidentate dpq/dppz ligands, two DMF and three $Cl^-$ anions. Crystal lattice shows intermolecular π-π stacking interactions between planar dpq and dppz ligands. Considering planarity and photosensitizing ability of the coordinated dpq and dppz ligands, complexes were studied for their binding interaction with DNA and protein and photo-induced DNA cleavage activity. They display significant binding propensity to the CT-DNA ($K_b$ ~$10^4$ $M^{-1}$) in the order **2**, **4** (dppz) >**1, 3** (dpq). Complexes **1**-**4** binds DNA through groove binding and partial intercalation. All the complexes also show binding propensity ($K_{BSA}$ ~ $10^5$ $M^{-1}$) to bovine serum albumin (BSA) protein. Complexes **1–4** efficiently cleave supercoiled (SC) ds-DNA to its nicked circular (NC) form on exposure to UV-A light of 365 nm via formation of singlet oxygen ($^1O_2$) and hydroxyl radical ($HO^•$) as reactive oxygen species in a photoredox pathway.

## Introduction

The trivalent Lanthanide (Ln) complexes have diverse applications in magnetic resonance imaging (MRI), luminescent bioprobes, sensing, luminescent MOF, single molecule magnet (SMM) because of their unique optical, structural and magnetic properties.[1-7] The fascinating optical and magnetic properties of Ln(III) originate from spatially shielded 4f orbitals from the ligand field. Ln(III) tend to favor high coordination numbers (CN > 6) owing to larger ionic sizes with nondirectional ionic bonding in nature. The commonly adopted coordination geometries were ranging from capped octahedral, dodecahedral, square antiprism, tricapped trigonal prism and bicapped dodechahedron. They form stable coordination complexes with a wide variety of polydentate ligands like polyaminocarboxylates (linear DTPA and cyclic DOTA), β-diketonates and macrocylic tetrapyrrole ligands.[8-10] Several Gd(III)- polyaminocarboxylate complexes like $[Gd(DTPA)(H_2O)]^{2-}$ (Magnevist) and $[Gd(DOTA)(H_2O)]^-$ (Dotarem) are predominant MR-contrast agents in commercial use.[3] Lanthanide emissions have unique features like very sharp emission bands, large Stokes' shift and long-lived excited state lifetimes compared to organic fluorophores.[2] Intrinsic luminescence of Ln(III) originate from f-f electronic transitions are Laporte forbidden thus resulting into weak luminescence and low molar absorptivity (ε). Attachment of light-harvesting organic chromophore as antenna to overcome this limitation by energy transfer to populate excited state of Ln(III).[11] In this context photoactivated chemotherapy (PACT) is a novel approach which offers a spatiotemporal control over drug activation having remarkable potential and advantages over conventional chemotherapy.[12]

In comparison to 3d-5d metal complexes, there are only few reports of photoactivated lanthanide complexes.[13,14] This lacuna provide an ample scope to explore photosensitized lanthanide complexes for therapy and diagnosis. The present work originate from our ongoing effort to explore the diverse structure and biological perspective of emissive Ln(III) complexes for their therapeutic applications.[15,16]

Herein, we present the synthesis, crystal structures, photophysical properties, binding with DNA and proteins and photo-triggered DNA cleavage activities of four Sm(III) and Er(III) complexes, viz. $[Sm(dpq)(DMF)_2(H_2O)Cl_3]$ (**1**), $[Sm(dppz)(DMF)_2(H_2O)Cl_3]$ (**2**), $[Er(dpq)(DMF)_2Cl_3]$ (**3**) and $[Er(dppz)_2Cl_3]$ (**4**) where dipyrido[3,2-d:2′,3′-f]quinoxaline (dpq

[a]*Department of Chemistry, Indian Institute of Technology Kanpur, Kanpur 208016, Uttar Pradesh, India. E-mail: akpatra@iitk.ac.in*

†Electronic Supplementary Information (ESI) available: Cyclic voltammograms; unit cell packing diagrams; selected bond distances and angles; DNA and protein binding plots; DNA cleavage data. For ESI and crystallographic data in CIF or other electronic format see DOI: 10.1039/x0xx00000x.

in **1** and **3**) and dipyrido[3,2-a:2′,3′-c]phenazine (dppz in **2** and **4**). The solid state structure of the complexes were determined by X-ray crystallography. They exhibit discrete mononuclear structures with eight coordinated distorted square

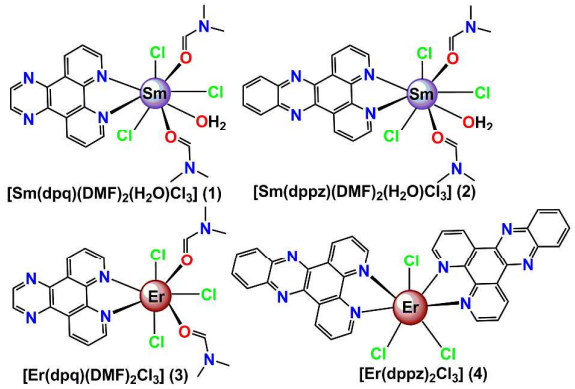


**Scheme 1** Samarium (III) and Erbium(III) complexes (**1**-**4**) studied in this work

antiprismatic geometry for **1** and **2** and seven-coordinated mono-capped octahedral geometry for **3** and **4**. Extended lattice structure showed significant π-π stacking interaction between planar heterocyclic bases and hydrogen bonding important to stabilize 2D-supramolecular sheet-like structures. Here dpq and dppz ligands act as photosensitizing antenna[17] to generate triplet excited states and thereby transfer energy to populate emissive Ln(III) excited states as well generate reactive oxygen species responsible for photo-induced oxidative damage of DNA.

## Results and discussion

### Synthesis and general aspects

Sm(III) and Er(III) complexes, viz. $[Sm(B)(DMF)_2(H_2O)Cl_3]$ (**1**), $[Sm(B)(DMF)_2(H_2O)Cl_3]$ (**2**), $[Er(B)(DMF)_2Cl_3]$ (**3**) and $[Er(B)_2Cl_3]$ (**4**) of *N*,*N*-donor heterocyclic bases (B), i.e. dipyrido[3,2-d:2′,3′-f]quinoxaline (dpq in **1** and **3**) and dipyrido[3,2-a:2′,3′-c]phenazine (dppz in **2** and **4**) are obtained in ~80% yield using a general synthetic procedure by reacting a methanolic solution of $SmCl_3·6H_2O$ or $ErCl_3·6H_2O$ with the corresponding *N*,*N*-donor bases (B) in boiling methanol. Complexes **1**-**4** were stable under ambient conditions, showed good solublity in DMF, DMSO, poor solubility in water, MeCN and alcohols and insoluble in $Et_2O$ and hydrocarbon solvents. The complexes were characterized from various spectroscopic and analytical techniques and solid state structure obtained from single crystal X-ray crystallography. Selected physicochemical data are given in Table 1. Time-dependent absorption spectral traces of the complexes in DMF at 298 K do not show any changes for 4 h suggest their stability in solution (Figs. S1, S2 in ESI†). The binding affinities ($K_{ML}$) of the ligands to Ln(III) were in the range of ~ $5\times10^4$ $M^{-1}$ as determined from fluorescence spectral titration studies (ESI†). The ESI-MS analysis of the complexes **1**-**4** showed respective molecular ion peaks in solution. The UV-visible spectra of the complexes in aqueous-DMF (9:1 v/v) show an intense ligand centered $\pi\rightarrow\pi^*$ transition at 272 nm (Fig. 1a). The dpq complexes exhibit a shoulder ~340 nm assigned to $n\rightarrow\pi^*$ transition involving the quinoxaline moiety. The dppz complexes **2** and **4** show two bands at 365 and 376 nm attributed to the $n\rightarrow\pi^*$ transitions of the phenazine moiety.[18]

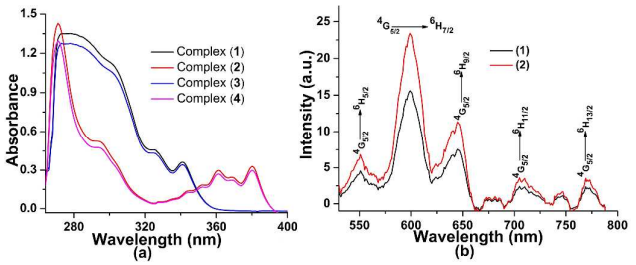


**Fig. 1** (a) UV-visible spectra of complexes **1**-**4** ([**1**], [**3**]: 100 μM; [**2**], [**4**]: 50 μM) in aqueous DMF at 298 K. (b) Time-delayed luminescence spectra of **1** (black) and **2** (red) in aqueous DMF, corresponding $^4G_{5/2} \rightarrow {}^6H_J$ transitions are shown on the respective spectra. Delay time = gate time = 0.1 ms, $\lambda_{ex}$ = 340 nm, $T$ = 298 K.

Complexes **1** and **2** showed characteristic emission bands for Sm(III) attributed to the $^4G_{5/2} \rightarrow {}^6H_J$ ($J$ =5/2, 7/2, 9/2, 11/2 and 13/2) f-f transitions, respectively[2] (Fig. 1b). The Er(III) complexes show typical emission at 545 nm due to $^4S_{3/2} \rightarrow {}^4I_{15/2}$ transition (Fig. S4, ESI†). The excited state lifetime of **1** and **2** were determined in $H_2O$ in $D_2O$ ($\tau$ = 0.14, 0.13 ms in $H_2O$) and ($\tau$ = 0.38 and 0.40 in $D_2O$) from the mono-exponential fitting of emission decay profile in aqueous media and the quantum yields are ($\phi_{overall}$ = 0.048, 0.056 in $H_2O$ and 0.320 and 0.422 in $D_2O$) respectively and details are given in Fig. S7, ESI†. The lower lifetime and quantum yield values in $H_2O$ compared to that in $D_2O$ is mainly due to the nonradiative quenching via O-H oscillators of $H_2O$ which lowers the excited state lifetime and thus emission quantum yields in solution. The excited state lifetimes of the complexes in degassed aqueous solutions are 2-3 times longer than that in the aerated solutions suggesting $O_2$ sensitivity on luminescence lifetime and excited state deactivation (ESI†).

The complexes were redox active primarily due to ligand centered reduction in DMF. The dpq complexes showed cathodic responses at -1.25 and -1.58 V with poor reversibility possibly due to instability of the reduced species. The dppz complexes show $E_{pc}$ at -1.14 and -1.08 V with $E_{pa}$ at -1.05 and -0.99V vs. Ag/AgCl with poor reversibility especially in complex **4** due to instability of reduced species following ECE mechanism (Figs. S8-10, ESI†). Similar observations were made earlier with analogous lanthanide complexes. [14a,15]

### X-ray crystal structures

The complexes **1**-**4**, *viz.* $[Sm(dpq/dppz)(DMF)_2(H_2O)Cl_3]$ (**1**, **2**), and $[Er(dpq)(DMF)_2Cl_3]$ (**3**) and $[Er(dppz)_2Cl_3]$ (**4**) were structurally characterized from single-crystal X-ray diffraction method. They exhibit discrete mononuclear species with the Sm(III) center in an eight coordinate $\{SmN_2O_3Cl_3\}$ polyhedra for **1** and **2** and Er(III) center in a seven-coordinate $\{ErN_2O_2Cl_3\}$ and $\{ErN_4Cl_3\}$ geometry for complexes **3** and **4** respectively (Figs. 2 and 3).

[Sm(dpq/dppz)(DMF)$_2$($H_2O$)$Cl_3$](**1, 2**) crystallizes in the triclinic space group $P\bar{1}$. Here each Sm(III) bound to one bidentate *N*,*N*-donor dpq or dppz ligand, two DMF molecules, one water and three chloride ligands in an eight-coordinate

| Complex | $\lambda_{max}$ [a] / nm, (ε/$M^{-1}cm^{-1}$) | $K_b$ [b] / $M^{-1}$ | $K_{app}$ [c] / $M^{-1}$ | $K_{BSA}$ [d] / $M^{-1}$ |
|---|---|---|---|---|
| **1** | 273 (12050), 324 (4170), 340 (3340) | 5.1 (±0.3) × $10^4$ | 1.09 × $10^6$ | 1.26(±0.1) x $10^5$ |
| **2** | 271 (25490), 360(5480), 380 (5980) | 7.7 (±0.2) × $10^4$ | 2.96 × $10^6$ | 2.17(±0.3) x $10^5$ |
| **3** | 272 (21580), 324 (7600), 340 (6180) | 5.7 (±0.3) × $10^4$ | 1.29 × $10^6$ | 1.98(±0.4) x $10^5$ |
| **4** | 272 (34550), 360 (12060), 380 (12880) | 9.6 (±0.4) × $10^4$ | 2.4 × $10^6$ | 1.62(±0.2) x $10^5$ |

**Table 1** Selected physicochemical data and DNA/BSA binding parameters for the complexes **1**-**4**

[a] UV-visible spectra in DMF. [b] $K_b$, intrinsic DNA binding constant. [c] $K_{app}$, apparent DNA binding constant. [d] $K_{BSA}$ , Stern-Volmer quenching constant for BSA fluorescence.

{$SmN_2O_3Cl_3$} coordination geometry. The ORTEP views of the complexes **1** and **2** are shown in Fig. 2. Such eight-coordinate polyhedron can be best described as distorted square antiprism (Figs. 4a, 4b).[19] The Sm-N (dpq/dppz) distances range from 2.662(2) Å to 2.678(2)Å for **1** and 2.643(3) Å to 2.687(3) Å for **2** respectively. The Sm-O(DMF), Sm-O($H_2O$) and Sm-Cl bond distances are 2.419(2) Å, 2.437(2)Å and 2.455(2) for **1** and 2.404(3) Å, 2.422(3)Å and 2.452(3) for **2**. ∠N-Sm-N bond angle are in the range of 60.84(10)-61.03(7)° and ∠Cl-Sm-Cl are in the range of 81.40(3)-90.92(3)° for complexes **1** and **2**. These values suggest that each Sm-Cl bond is nearly perpendicular to each other. The complexes exhibit strong favorable interpenetrable $\pi$-$\pi$ stacking interactions (interplanar distance ~3.628 Å) within bound dpq/dppz ligands of neighbouring molecule in the three-dimensional extended crystal lattice[20a] (Figs. 5a, 5b). These structures also demonstrate intermolecular bifurcated hydrogen bonding between hydrogen atoms of the bound water molecule with two coordinated chlorides of neighboring molecules in a crystal lattice with O-H….Cl distances of 2.347(3) Å and 2.460(9) Å (Fig. 5d).[20b] These supramolecular noncovalent interactions stabilize the crystal lattice structure in 3D in solid state.

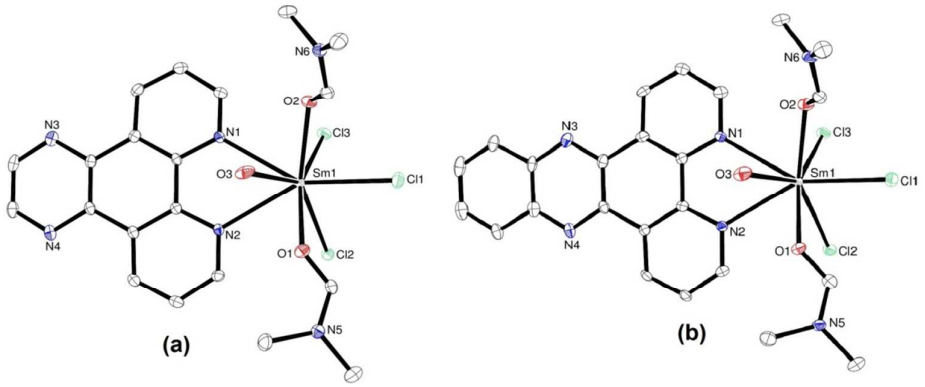


**Fig. 2** ORTEP view of (a) [Sm(dpq)(DMF)$_2$($H_2O$)$Cl_3$] (**1**) and (b) [Sm(dppz)(DMF)($H_2O$)$Cl_3$] (**2**), showing 50% probability thermal ellipsoids and the atom numbering scheme for the metal and heteroatoms. The hydrogen atoms were omitted for clarity.

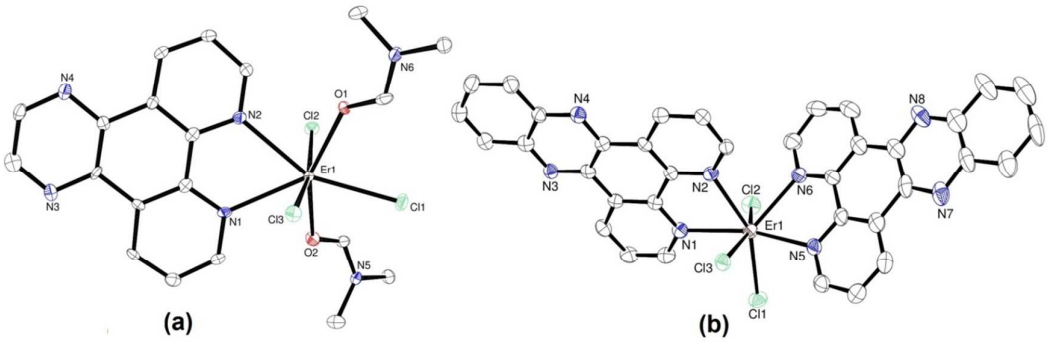

Journal Name

ARTICLE

**Fig. 3** ORTEP view of (a) $[Er(dpq)(DMF)_2Cl_3]$ (**3**), and (b) $[Er(dppz)_2Cl_3]$ (**4**), showing 50% probability thermal ellipsoids and the atom numbering scheme for the metal and heteroatoms. The hydrogen atoms were omitted for clarity.

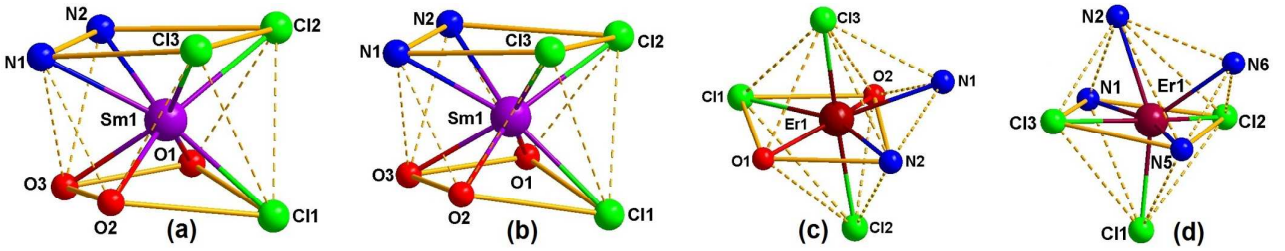


**Fig. 4** Coordination polyhedra of the lanthanide cores for the complexes showing distorted square antiprism geometries for **1** (a), **2** (b) and distorted mono-capped octahedron geometries for **3** (c) and **4** (d).

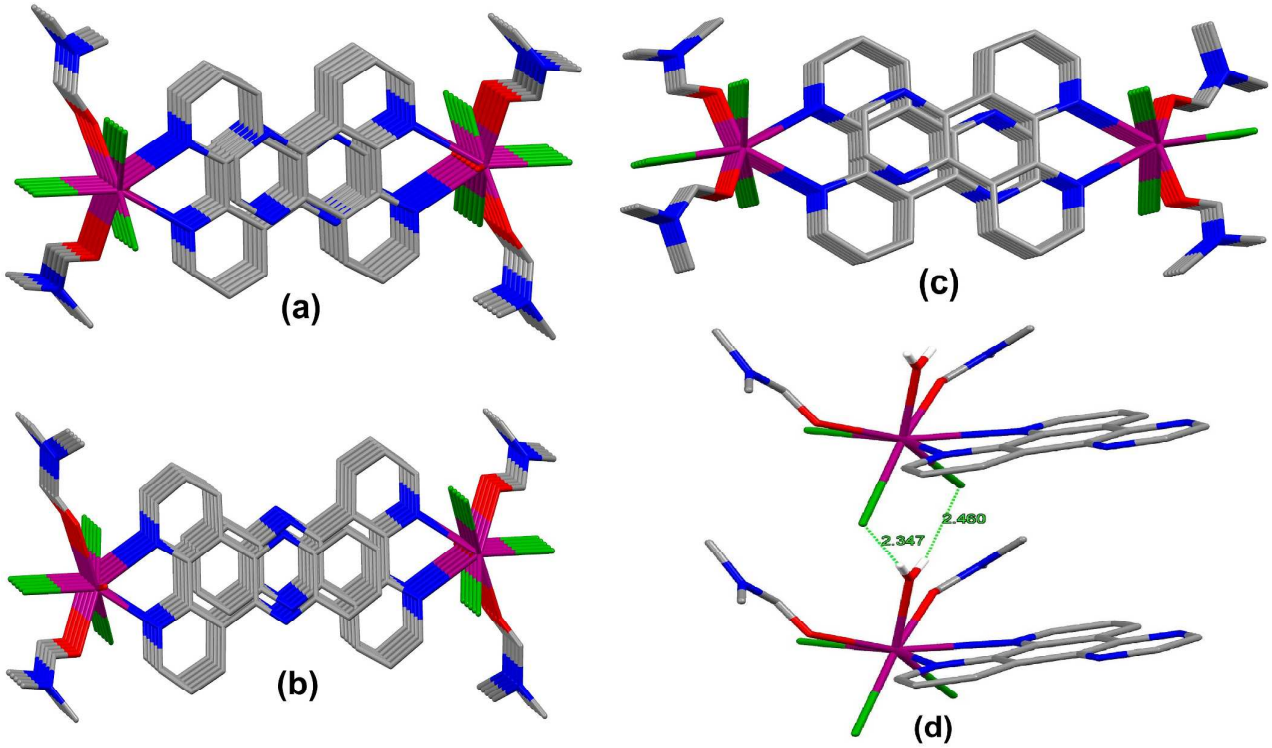


**Fig. 5** (a)-(c) Interpenetrating π-π stacking interactions between planar heterocyclic bases of neighboring molecules to form 2D supramolecular sheet in complexes **1**-**3** respectively. (d) Bifurcated hydrogen bonding interactions in $[Sm(dpq)(DMF)_2(H_2O)Cl_3]$ (**1**) originate from Sm(III)-bound $H_2O$ with two chlorides of neighboring molecule.

Selected bond lengths and angles are given in Table S1 in ESI†. The unit cell packing diagrams for the complexes **1** and **2** are given in Fig. S11 in ESI†.

$[Er(dpq)(DMF)_2Cl_3]$ (**3**) and $[Er(dppz)_2Cl_3]$ (**4**) crystallizes in triclinic space group $P\bar{1}$ and orthorhombic space group *Pccn*. The asymmetric units of the complexes contain two and eight independent molecules respectively. In complex **3,** Erbium is seven-coordinated $\{ErN_2O_2Cl_3\}$ coordination geometry comprising of two nitrogen atoms of a bidentate dpq ligand, two oxygen atoms of two DMF ligands and three chloride ligands. In complex **4** the Erbium center also shows a seven-coordinate $\{ErN_4Cl_3\}$ coordination geometry originated from

two bidentate *N,N'*-donor dppz ligands and three chloride ligands. The ORTEP diagrams of the complexes **3** and **4** are shown in Fig. 3. Such seven-coordinate coordination polyhedra in complexes **3** and **4** could be best described as distorted mono-capped octahedron or distorted octahedral wedge geometry (Figs. 4c, 4d).[21] The Er-N (dpq/dppz) bond distances in complexes are in the range of 2.519(13) to 2.558(13)Å in **3** and from 2.479(3) to 2.509(3)Å in **4** respectively. Er-O(DMF) and Er-Cl bond distances in complex **3** are in the range of 2.299(10) to 2.303(11) Å and 2.588(4) to 2.645(4) Å, where as Er-Cl bond distances in complex **4** ranges from 2.5655(11) to 2.6124(12) Å respectively.

The unit cell packing diagrams for the complexes are given in Fig. S12 in ESI†. The Er-dpq complex **3** shows favourable interpenetrable $\pi$-$\pi$ stacking interactions (interplanar distance ~4.145 Å) as observed for complexes **1** and **2** in extended crystal lattice forming 2D supramolecular sheet, whereas this is not feasible for complex **4** due to presence of two planar dppz rings bound to Er(III) at a dihedral angle of ~55$^0$ preventing such $\pi$-$\pi$ stacking interactions (Fig. S13, ESI†). Selected bond lengths and angles are given in Table S2 in ESI†.

**Thermogravimetric (TGA) and powder X-ray diffraction (PXRD) analyses**

Thermogravimetric analysis (TGA) was done to explore the thermal stability of **1–4** (Fig. 6a). The TGA profile of **1** and **2** exhibit similar thermal behavior. The TGA diagram showed that complexes were thermally stable upto ~ 200 °C and then shows a first weight loss of 3% attributed to the loss of coordinated water molecule (calcd: 2.5 wt%) followed by major and sharp weight loss near 350 $^0$C corresponding to the loss of the coordinated organic ligands and chloride ions, leaving a residual weights of ~26%. TGA curve of **3** shows that it is stable up to ~100 $^0$C followed by minor weight loss of ~14% upto 260 $^0$C attributed to the loss of coordinated DMF molecules and subsequently, a major sharp weight loss at 380 $^0$C is observed for loss of dpq and chloride leaving a residual weight of 30%. The TGA profile of **4** indicates it is thermally stable up to ~90 $^0$C after which showed a 17% weight loss corresponding to three chloride ions and after 380 $^0$C, a rapid weight loss is observed due to loss of dppz ligands with residual weight of 31%. The differences in TGA profiles of **3** and **4** may originate from their structural difference in coordination polyhedra and stability in solid state**.** Thermal stability of the complexes **1** and **2** were also confirmed from powder X-ray diffraction (PXRD) data(Fig. 6b, 6c) showing these complexes are thermally stable upto 200 $^0$C.

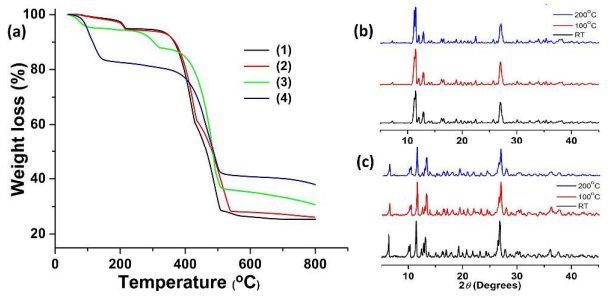


**Fig. 6** (a) TGA plots for complexes **1**-**4** under $N_2$ atmosphere with a heating rate of 10 $^0$C min$^{-1}$. Temperature dependent PXRD data of complex **2** (b) and **1** (c).

**DNA binding studies**

**Absorption spectral studies.** Complexes of phenathroline bases coordinated transition metals were explored for their DNA recognition, charge-transfer to nucleic acid, as foot printing reagents and as photoactivated chemotherapeutic agents.[22] This prompted us to study the binding interactions of Ln-dpq/dppz complexes with DNA and proteins. The UV-vis titrations were carried out to determine the binding affinity of the complexes to CT-DNA (Fig. 7a, Figs. S17-S19, ESI†). The binding of **1**-**4** to DNA results in significant hypochromism in absorption band due to partial interaction/charge transfer interaction between complexes and the DNA base pairs.[23] The intrinsic binding constants ($K_b$) between complexes and CT-DNA are given in Table 1. The $K_b$ values follow the order:**2**≈**4** (dppz) >**1**≈**3** (dpq) is because of higher binding affinity of dppz complexes (**2**, **4**) due to an extended planar aromatic moiety which intercalate strongly with the base pairs in DNA.

**Ethidium bromide (EthB) displacement assay.** EthB acts as spectral probe by enhanced emission intensity when intercalatively bound to DNA and reduced emission intensity in free state in buffer medium due to solvent quenching.[24] The competitive binding of **1**-**4** to DNA could result in displacement of the bound EthB by complexes was monitored by changes in emission intensity of EthB pretreated CT-DNA with increasing [complex].[25] The relative apparent binding constants ($K_{app}$) of the complexes **1**-**4** to CT-DNA was determined by this study (Table 1, Fig. 7b, Figs. S20-S22, ESI†).The $K_{app}$ values of the complexes are ~$10^6$ M$^{-1}$ and follow the order of **2** ≈ **4** (dppz) > **1** ≈ **3** (dpq). Thus the higher values of $K_b$ and $K_{app}$ of studied Ln(dpq/dppz) complexes revealed good binding affinity to CT-DNA possibly through DNA groove binding and partial intercalative mode.

**BSA binding studies.** The binding affinity of complexes **1**-**4** with bovine serum albumin (BSA) were studied using intrinsic tryptophan emission quenching of BSA in presence of the complexes.[26a] Upon increase in concentration of the complexes **1**-**4**, the emission intensity of BSA at 345 nm decreases steadily (Fig. 7c). The quenching of emission can result from various molecular interactions arises due to changes in BSA secondary structure upon binding of the complexes including subunit association, substrate binding, or conformation changes of the protein.[26b] The Stern-Volmer quenching constant ($K_{BSA}$) for complexes **1**-**4** have been calculated from slope of the linear plot of $I_0/I$ vs. [complex] using Stern-Volmer equation[27] (Figs. S23–S25, ESI†) and corresponding values are listed in Table 1. The $K_{BSA}$ values of ~$10^5$ M$^{-1}$ indicate that the complexes favorably bind to serum proteins.

Journal Name

ARTICLE

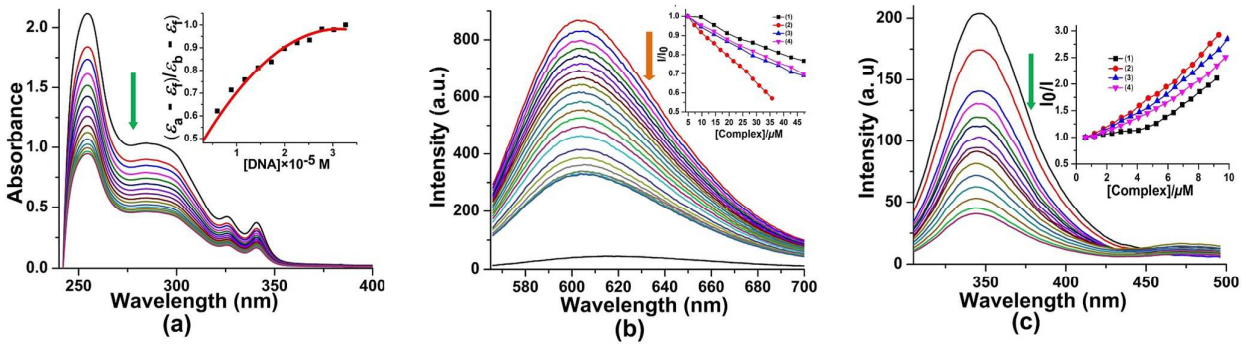


**Fig. 7** (a) UV-vis traces of [Sm(dpq)(DMF)$_2$(H$_2$O)Cl$_3$] (**1**) ) (50 $\mu$M) in 5 mM Tris-HCl/NaCl buffer (pH 7.2) with increasing [CT-DNA] at 298 K. The inset shows $\Delta\varepsilon_{af}/\Delta\varepsilon_{bf}$ *vs.* [DNA] plot for complex **1**. (b) Emission spectral traces of EthB bound CT-DNA with increasing [**1**] in 5 mM Tris-HCl/NaCl buffer (pH 7.2) 298 K. $\lambda_{ex}$= 546 nm, $\lambda_{em}$ = 603 nm, [DNA] = 313 $\mu$M, [EthB] = 12 $\mu$M. The inset shows the plot of $I/I_0$ *vs.* [complex] for the complexes.**1** -**4**. (c) The effect of addition of complex **2** on the fluorescence quenching of BSA in 5 mM Tris-HCl/NaCl buffer at 298 K (pH 7.2).$\lambda_{ex}$ = 295 nm, $\lambda_{em}$= 340 nm, [BSA] = 5 $\mu$M. The Inset shows the plot of $I_0/I$ *vs.* [complex] for the complexes **1**-**4**.

### DNA photocleavage activity

The photo-induced DNA cleavage activities of the complexes **1**-**4** was studied using supercoiled (SC) pUC19 DNA by exposing the samples with low power UV-A light of 365 nm (6 W) (Fig. 8). The complexes containing photoactive dpq and dppz ligands show significant DNA photocleavage activity through generation of photoexcited $^3(n\text{-}\pi^*)$ and/or $^3(\pi\text{-}\pi^*)$ states. Although there remains differences in absorbances for dpq and dppz complexes, the photosensitizing ability of dpq is significantly greater than dppz due to efficient delocalization of nonbonding electrons through additional benzene ring present in dppz. The complexes **1**-**4** (20 $\mu$M) on photoexcitation at 365 nm for 2 h showed ~85-95% conversion to nicked circular (NC) form. Control experiments clearly reveal absence of DNA hydrolytic cleavage in dark (L6-L9 in Fig. 8). The extent of photocleavage increases with increasing concentration of the complexes and exposure time (Figs. S26, S27 in ESI†). The DNA groove binding studies of the complexes were studied using the DNA major groove binder methyl green (MG).

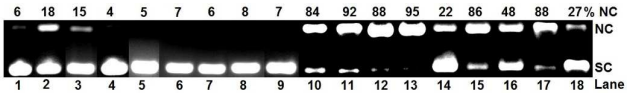


**Fig. 8** Photocleavage of SC pUC19 DNA (0.2 $\mu$g) with complexes **1**-**4** and controls (20 $\mu$M ) in 50 mM Tris-HCl buffer (pH, 7.2) at 37 $^0$C for 1 h on exposure with UV-A light of 365 nm (6 W) for 2 h: L1, DNA control; L2, DNA + dpq; L3, DNA + dppz; L4, $SmCl_3$ control; L5, $ErCl_3$ control; L6, DNA + **1** (dark); L7, DNA + **2** (dark); L8, DNA + **3** (dark); L9, DNA + **4** (dark); L10, DNA + **1**; L11, DNA + **2**; L12, DNA + **3**; L13, DNA + **4**; L14, DNA + methyl green (MG); L15, DNA + **1** + MG; L16, DNA + **2** + MG; L17, DNA + **3** + MG; L18, DNA + **4** + MG.

MG pretreated SC-DNA with dppz complexes shown significant inhibition of photocleavage activity whereas dpq complexes display no apparent inhibition. This suggests minor groove binding preference for the dpq (**1** and **3**) and major groove binding preference for the dppz (**2** and **4**) complexes respectively.

The mechanistic investigations DNA photocleavage reactions were carried in the presence of various external reagents like $NaN_3$ and L-histidine as $^1O_2$ quenchers[28] and DMSO, catalase and KI as $^{\bullet}$OH radical scavengers (Figs. S28 – S30 in ESI†).[29,30] Addition of $^1O_2$ quenchers and $^{\bullet}$OH scavengers results into partial and moderate inhibition of photo-induced DNA cleavage activity of the complexes. The enhancement of photoclevage activity in $D_2O$ due to longer lifetime of $^1O_2$ than that in $H_2O$.[31] These results are suggestive towards involvement of both $^1O_2$ and $^{\bullet}$OH radicals as cleavage active ROS involving both type-II and photoredox pathways observed earlier from analogous Ln(III) complexes.[13-15]

## Experimental

### Materials and methods

Commercially available solvents and reagents were purchased and used as received and solvents were purified by standard procedure.[32] 1,10-phenanthroline (phen), 1,2-diaminobenzene, ethylene diamine, $SmCl_3{\cdot}6H_2O$, $ErCl_3{\cdot}6H_2O$, calf thymus (CT) DNA, bovine serum albumin (BSA, fraction V), agarose (molecular biology grade), methyl green, catalase, ethidium bromide (EthB), gel loading solution (containing 0.25% (w/v) bromophenol blue, 0.25% xylene cyanol FF and 40% sucrose in water) were purchased from Sigma-Aldrich. Supercoiled (SC) plasmid pUC19 (CsCl purified) was purchased from Merck Millipore. Tris-(hydroxymethyl)-aminomethane-HCl (Tris-HCl)

buffer solution was prepared using Milli-Q water (18.2 MΩ). dipyrido-[3,2-d:2′,3′-f]-quinoxaline (dpq) and dipyrido[3,2-a:2′,3′-c]phenazine (dppz) were synthesized according previously reported method.[33,34] The elemental microanalyses and infrared spectra were recorded on a Perkin-Elmer 2400 Series-II elemental analyzer instrument and a Perkin-Elmer model 1320 FT-IR spectrometer in KBr pellets in the 4000-400 cm-1 range. Electronic spectra were recorded in Perkin-Elmer Lambda 25 spectrophotometers. Thermo gravimetric analyses were carried out under $N_2$ atmosphere with a heating rate of 10 °C $min^{-1}$ using a Mettler Toledo Star System. Powder X-ray diffraction (PXRD) data were collected on a PANalytical X'Pert Pro X-ray diffractometer with Cu Kα radiation (λ= 1.540598 Å) with a scan rate of 3° $min^{-1}$ at 293 K, 373 K and 473 K. Electrospray ionization mass spectral (ESI-MS) measurements were carried out using a WATERS Q-TOF Premier mass spectrometer. Agilent Cary Eclipse fluorescence spectrophotometer were used to record the fluorescence and time-delayed luminescence spectra of **1**-**4** at 298 K. Lifetime measurements for Sm(III) complexes were performed under ambient conditions using a pulsed Xenon lamp at $\lambda_{ex}$ = 340 nm, 380 nm and $\lambda_{em}$ = 598 nm for Sm(III) with a delay time and gate time of 0.1 ms. Decay curves were fitted by non-linear least square method. The overall quantum yields of the complexes were measured in $H_2O$ and $D_2O$ at room temperature according to known literature procedure using quinine sulfate as reference using following equation:[27]

$$\emptyset_{\text{overall}} = \emptyset_{\text{ref}} \frac{A_{\text{ref}} In^2}{A I_{\text{ref}} n_{\text{ref}}^2}$$

Where A, I and n denote the respective absorbance at the excitation wavelength, area under the emission spectral curve and refractive index of the solvent respectively. The $\phi_{\text{ref}}$ represents the quantum yield of the standard quinine sulfate solution. The binding affinity of the dpq and dppz ligands with lanthanide ions were determined using fluorescence titration method with the increasing concentration of the respective ligands to the Ln(III) (ESI†).

**Synthesis and characterization**

**Synthesis of complexes 1-4.**

$SmCl_3 \cdot 6H_2O$ (0.200 g; 0.548 mmol) and $ErCl_3 \cdot 6H_2O$ (0.200 g; 0.523 mmol) were dissolved in 10 mL methanol under stirring. To this methanolic solution, a hot methanolic solution (20 mL) of the respective heterocyclic bases (dpq/dppz) [0.127 g dpq, 0.548 mmol (**1**); 0.309 g dppz; 0.548 mmol (**2**); 0.121 g dpq, 0.523 mmol (**3**) and 0.295 g dppz, 1.047 mmol (**4**)] was added dropwise and the reaction was continued for 4 h in water bath at 60 $^0$C to obtain the desired product as precipitate which was filtered and successively washed with hot methanol (2 x 5 mL), diethyl ether (2 x 5 mL), and finally dried in vacuum over $P_4O_{10}$ [Yield: ~80%]. On layering of the compounds dissolved in DMF with $Et_2O$ at RT, suitable crystals were obtained for X-ray crystallography. The characterization data for the complexes are given below.

**[Sm(dpq)(DMF)$_2$(H$_2$O)Cl$_3$] (1).** Yield: 0.287 g (80%). Anal. calc. for $C_{20}H_{24}Cl_3N_6O_3Sm$: C, 36.78; H, 3.70; N, 12.87 Found: C, 36.63; H, 3.61; N, 12.72. ESI-MS (in DMF): m/z 792.13 $[M+2H_2O+H]^+$. Calcd: *m/z* 792.04. FT-IR (KBr, $cm^{-1}$): 3201(w, br), 3078(w), 1581(s), 1527(s), 1475(s), 1424(s), 1397(vs), 1337(s), 1304(s) 1242(s), 1209(m), 1118(s), 1081(vs), 1055(s), 995(s), 884(m), 835(s), 820(s), 812(s), 737(vs), 695(s), 634(s) (vs, very strong; s, strong; m, medium; w, weak; br, broad). UV-visible in DMF [λ, nm ($\varepsilon$, $M^{-1}cm^{-1}$)]: 340 (3340), 324 (4170), 273 (12050). Molar conductance in aqueous DMF (1:9) at 298 K ($\Lambda_M$): 96 S $cm^2$ $M^{-1}$.

**[Sm(dppz)(DMF)$_2$(H$_2$O)Cl$_3$] (2).** Yield: 0.298 g (77%). Anal. calc. for $C_{24}H_{26}Cl_3N_6O_3Sm$: C, 40.99; H, 3.73; N, 11.95. Found: C, 40.86; H, 3.62; N, 11.84. ESI-MS (in DMF): m/z 703.03 ($[M]^+$, 100%). Calcd: *m/z* 703.03. FT-IR (KBr, $cm^{-1}$): 3487(w), 3236(w,br), 3089(w), 1577(s), 1493(vs), 1464(m), 1412(s), 1362(vs), 1337(m), 1316(m), 1229(s), 1184(m), 1127(s), 1077(vs), 1042(s), 990(s), 815(s), 763(s), 735(vs), 702(m), 636(s), 616(s). UV-visible in DMF [λ, nm ($\varepsilon$, $M^{-1}cm^{-1}$)]: 379 (5980), 360 (5480), 271 (25490). Molar conductance in aqueous DMF (1:9) at 298 K ($\Lambda_M$): 88 S $cm^2$ $M^{-1}$.

**[Er(dpq)(DMF)$_2$Cl$_3$] (3).** Yield: 0.288 g (84%). Anal. calc. for $C_{20}H_{22}N_6O_2Cl_3Er$: C, 36.84; H, 3.40; N, 12.89. Found: C, 36.72; H, 3.32; N, 12.73. ESI-MS (in DMF-MeOH): *m/z* 719.21 $[M+MeOH+2H_2O]^+$, calcd: m/z 719.08, FT-IR (KBr, $cm^{-1}$): 3218(w, br), 1639(w), 1577(s), 1528(s), 1479(s), 1401(vs), 1389(vs), 1336(m), 1265(m), 1208(s), 1116(s), 1082(s), 1052(m), 872(s), 835(m), 812(vs), 736(vs), 701(s), 638(s). UV-visible in DMF [λ, nm ($\varepsilon$, $M^{-1}cm^{-1}$)]: 340(6180), 324(7600), 272 (21580). Molar conductance in aqueous DMF (1:9) at 298 K ($\Lambda_M$): 83 S $cm^2$ $M^{-1}$.

**[Er(dppz)$_2$Cl$_3$] (4).** Yield: 0.349 g (79%). Anal. calc. for $C_{36}H_{20}N_8Cl_3Er$: C, 51.58; H, 2.40; N, 13.37.Found: C, 51.43; H, 2.28; N, 13.26. ESI-MS (in DMF-MeOH): *m/z* 869.25 $[M+MeOH]^+$, calcd: m/z 869.05, FT-IR (KBr, $cm^{-1}$): 3357 (w,br), 2925(br), 1633(w), 1578(m), 1524(m), 1491(s), 1465(m), 1416(s), 1362(s), 1337(s), 1231(m), 1133(s), 1077(s), 1045(s), 817(s), 763(s), 738(vs), 708(s), 636(s), 617(s). UV-visible in DMF [λ, nm ($\varepsilon$, $M^{-1}cm^{-1}$)]: 379sh (12880), 360 (12060), 272 (34550). Molar conductance in aqueous DMF (1:9) at 298 K ($\Lambda_M$): 89 S $cm^2$ $M^{-1}$.

**Solubility and Stability.** Synthesized **1**-**4** complexes were highly soluble in DMF and DMSO and less soluble in MeOH, EtOH and MeCN. The complexes were stable in solid state and in solution under the experimental conditions.

**Single-crystal X-ray structure determination**

Structural determination of Complexes **1**-**4** were done by single-crystal X-ray diffraction technique. Suitable Single crystals of **1**-**4** were mounted on a glass fiber and used for data collection. All geometric and intensity data were collected on a Bruker D8 Quest Microfocus X-Ray CCD diffractometer equipped with an Oxford Instruments low-temperature attachment, with graphite-monochromated Mo Kα radiation ($\lambda$ = 0.71073 A°) at 100(2) K using $\omega$-scan technique (width of 0.5° per frame) at a scan speed of 10 s per frame controlled by manufacturer's APEX2 v2012.4-3 software package.[35] Intensity

data, collected using $\omega$-2$\theta$ scan mode, were corrected for Lorentz-polarization effects,[36] processed and integrated with Bruker's SAINT software. Multiscan absorption corrections were applied with the SADABS program.[37] The space group was determined using XPREP. The structures were subsequently solved by the direct methods using SHELXS-97[38] and was refined on $F^2$ by full-matrix least-squares technique using the SHELXTL 6.14 software package.[39] The structures were further refined and processed with the SHELXL-97 incorporated into the WinGX1.70 crystallographic package.[40] All non-hydrogen atoms were refined anisotropically till convergence is reached. All the hydrogen atoms were included in idealized positions and

| Parameters | [Sm(dpq)(DMF)$_3$(H$_2$O)Cl$_3$] (**1**) | [Sm(dppz)(DMF)$_3$(H$_2$O)Cl$_3$] (**2**) | [Er(dpq)(DMF)$_3$Cl$_3$] (**3**) | [Er(dppz)$_2$Cl$_3$] (**4**) |
|---|---|---|---|---|
| Empirical formula | $C_{20}H_{24}Cl_3N_6O_3Sm$ | $C_{24}H_{24}Cl_3N_6O_3Sm$ | $C_{20}H_{22}Cl_3ErN_6O_2$ | $C_{36}H_{20}Cl_3N_8Er$ |
| $M_r$ | 653.15 | 703.21 | 652.05 | 838.21 |
| crystal system | Triclinic | Triclinic | Triclinic | orthorhombic |
| space group | *P*-1 | *P*-1 | *P*-1 | *Pccn* |
| a (Å) | 7.0536(19) | 7.0374(7) | 7.8039(8) | 21.540(4) |
| *b* (Å) | 9.661(3) | 9.4788(10) | 12.3957(13) | 17.225(3) |
| *c* (Å) | 18.080(5) | 20.619(2) | 12.9005(14) | 19.377(4) |
| $\alpha$ (deg) | 84.809(5) | 93.687(3) | 75.916(2) | 90 |
| $\beta$ (deg) | 78.965(5) | 99.462(3) | 75.023(2) | 90 |
| $\gamma$ (deg) | 80.563(5) | 98.885(2) | 82.220(2) | 90 |
| Volume (Å$^3$) | 1190.7(5) | 1334.7(2) | 1165.8(2) | 7189(2) |
| *Z* | 2 | 2 | 2 | 8 |
| $D_x$ (Mg m$^{-3}$) | 1.822 | 1.750 | 1.858 | 1.549 |
| $\mu$ (mm$^{-1}$) | 2.838 | 2.539 | 3.973 | 2.595 |
| *F*(000) | 646 | 698 | 638 | 3288 |
| *T* (K) | 100(2) | 100(2) | 100(2) | 100(2) |
| $\theta$ range for data collection (deg) | 2.14 to 26.00° | 2.01 to 26.00° | 2.11 to 25.25° | 2.31 to 28.08 |
| Limiting indices | -8≤*h* ≤ 8<br>-11 ≤*k* ≤ 11,<br>-22 ≤*l* ≤ 19 | -8≤*h* ≤ 8<br>-11 ≤*k* ≤ 11,<br>-25≤*l* ≤25 | -9≤*h* ≤9<br>-14≤*k* ≤ 11,<br>-15≤*l* ≤ 15 | -28≤*h* ≤ 17<br>-22 ≤*k* ≤ 22,<br>-25 ≤*l* ≤ 25 |
| Reflections collected | 8594 | 16894 | 7441 | 43118 |
| unique reflections | 4666 | 5266 | 4055 | 6336 |
| *R*(int) | 0.0293 | 0.0432 | 0.0404 | 0.0408 |
| $T_{max}$ / $T_{min}$ | 0.6441/ 0.5872 | 0.6722/ 0.6177 | 0.5349 /0.4892 | 0.556/0.595 |
| Data/restraints/parameters | 4666 / 3 / 307 | 5266 / 0 / 338 | 4055 / 6 / 287 | 6336/0/433 |
| GOF on $F^2$ | 1.093 | 1.194 | 1.381 | 1.049 |
| $R_1$[a] and $wR_2$[b] [$I>2\sigma(I)$] | 0.0254, 0.0618 | 0.0297, 0.0755 | 0.0652, 0.2077 | 0.0343, 0.0825 |
| $R_1$ and $wR_2$ (all data) | 0.0280, 0.0630 | 0.0375, 0.0928 | 0.0679, 0.2089 | 0.0445, 0.0872 |
| Largest diff. peak and hole (e.A$^{-3}$) | 0.765 and -0.611 | 1.279 and -0.868 | 5.582 and -1.633 | 1.48 and -0.44 |

**Table 2.**Selected crystallographic data and structure refinement parameters for the complexes **1**-**4**

[a]$R_1=\Sigma||F_o|-|F_C||/\Sigma|F_0|$; [b]$wR_2=\{\Sigma[w(F_o^2-F_C^2)]/\Sigma[w(F_0^2)^2]\}^{1/2}$

refined using a riding model. Selected crystallographic data and refinement parameters for complexes **1**-**4** are summarized in Table 2. Perspective views of the complexes were obtained using ORTEP.[41] The CCDC deposition numbers for the complexes **1**-**4** are 1439892-1439895 respectively.

**DNA binding experiments**

Calf thymus (CT) DNA in 5 mM Tris-HCl/NaCl buffer (pH 7.2) gave $A_{260}$/ $A_{280}$ of 1.8-1.9, indicating that DNA is apparently free from protein.[42] The concentration of CT-DNA was determined from its $A_{260}$ value with a known molar extinction coefficient ($\varepsilon_{260}$) of 6600 $M^{-1}cm^{-1}$.[43] Absorption spectral titration experiments were made by varying the concentration of the CT-DNA while maintaining a constant complex concentration. Due corrections was made for the absorbance of CT DNA itself. The intrinsic equilibrium DNA binding constant ($K_b$) of **1**-**4** was obtained using the equation

$[DNA]/(\varepsilon_a-\varepsilon_f) = [DNA]/(\varepsilon_b-\varepsilon_f) + 1/ K_b(\varepsilon_a-\varepsilon_f)$

Where [DNA] is the concentration of DNA in the base pairs, $\varepsilon_a$ is the apparent extinction coefficient observed for the complex, $\varepsilon_f$ corresponds to the extinction coefficient of the complex in its free form, and $\varepsilon_b$ refers to the extinction coefficient of the complex when fully bound to DNA.[44]

The competitive binding assay from ethidium bromide (EthB) displacement were performed in 5 mM Tris-HCl/NaCl buffer (pH 7.2) by measuring emission intensities of a EthB bound CT-DNA with gradual increase of [complex]. The emission intensities of EthB at 603 nm ($\lambda_{ex}$ = 546 nm) were recorded after each addition of the complex. The apparent

binding constants ($K_{app}$) values were obtained from the equation: $K_{app}$ x $C_{50}$ = $K_{EthB}$ x [EthB], where $K_{app}$ is the apparent binding constant of the complex studied, $C_{50}$ is the [complex] at 50% quenching of DNA-bound EthB emission intensity, $K_{EthB}$ is the binding constant of EthB ($K_{EthB}$ = 1 x $10^7$ $M^{-1}$), and [EthB] = 12 $\mu$M.[45]

**Protein binding experiments**

The complex solutions were gradually added to the solution of BSA (5 μM) in 5 mM Tris-HCl-NaCl buffer (pH 7.2) and the quenching of the emission signals at 340 nm ($\lambda_{ex}$ = 295 nm) were recorded. The quenching constant ($K_{BSA}$) has been determined quantitatively by using Stern-Volmer equation.[27] Stern-Volmer plots for $I_0/I$ vs. [complex] were made using the corrected fluorescence data taking into account the effect of dilution. Linear fit of the data using the equation: $I_0/I = 1 + K_{BSA}[Q]$, where $I_0$ and $I$ are the emission intensities of BSA in the absence of quencher and in the presence of quencher of concentration [Q], gave the quenching constants ($K_{BSA}$).

**DNA cleavage experiments**

The cleavage of SC pUC19 (30 μM, 0.2 μg, 2686 base pairs) in presence of complexes was performed in Tris-HCl/NaCl buffer (50 mM, pH 7.2) by photo-irradiation using UV-A light of 365 nm (6 W, Model VL-6.LC from Vilber Lourmat, France) by agarose gel electrophoresis. Mechanistic studies were performed using different additives as ROS scavengers/quenchers ($NaN_3$, 400 $\mu$M; KI, 200 $\mu$M; L-histidine, 200 $\mu$M; DMSO, 2 $\mu$L; catalase, 4 units) prior to the addition of the complexes. To investigate the effect of $D_2O$ on DNA photocleavage, $D_2O$ was added for dilution of the sample to 20 $\mu$L. After incubation of the sample at 37 °C for 1 h in dark and quenched by gel loading dye, solution was loaded on 1% agarose gel having 1 $\mu$g/mL ethidium bromide. Electrophoresis was run for 2.0 h at 60 V in Tris-acetate EDTA (TAE) buffer (pH 8.1) in dark room. The quantification of cleavage products was performed using UVITEC FireReader V4 gel documentation system and UVI band software. The error observed in measuring the band intensities was in the range of 4-7%.

## Conclusions

In conclusion, we have synthesised and structurally characterized a new series of luminescent samarium(III) and erbium(III) complexes containing *N*,*N*-donor phenanthroline bases. The single crystal X-ray diffraction analyses reveal that the complexes **1**-**4** are mononuclear in nature. The Sm(III) complexes (**1**, **2**) showed eight coordinate {$SmN_2O_3Cl_3$} core having distorted square antiprismatic geometry around Sm(III). The Er(III) complexes showed seven-coordinate {$ErN_2O_2Cl_3$} and {$ErN_4Cl_3$} mono-capped octahedral geometry around Er(III) for **3** and **4** respectively. These structures are stabilized in 3D crystal lattice by supramolecular non-covalent interactions like strong favorable interpenetrable $\pi$-$\pi$ stacking interactions within bound dpq/dppz ligands, and bifurcated hydrogen bonding between hydrogens of coordinated water of the Sm(III) to the coordinated chloride ions of the neighbouring molecule. The thermal stability of these complexes was studied by thermogravimetric and powder XRD analyses. The efficient light harvesting ability of dpq/dppz coordinated samarium complexes **1**-**2** evidenced from their luminescence in visible region with low to moderate lifetimes in ms and quantum yields. In addition, the complexes showed good binding propensity with DNA by groove binding and partial intercalation through planar dpq/dppz bases. The complexes **1**-**4** exhibit efficient photo-induced DNA cleavage activity at low power UV-A light of 365 nm following $^1O_2$ and $^{\bullet}OH$ radical in a photoredox pathway at micromolar concentration. Further studies are on to develop visible and NIR luminescent lanthanide based materials for potential bioresponsive applications.

## Acknowledgements

We thank IIT Kanpur for startup grant and Science and Engineering Research Board (SERB), Govt. of India, (SB/FT/CS-062/2012) for financial support. S.D., Z.A., P. K. thank IIT Kanpur and UGC for their research fellowships.

## Notes and references

1 S. Cotton, *Lanthanides and actinide chemistry*, John Wiley & Sons Ltd., England, 2006.
2 (a) J.-C. G. Bünzli, *Chem. Rev.*, 2010, **110**, 2729-2755; (b) S. V. Eliseeva and J.-C. G. Bünzli, *Chem. Soc. Rev.*, 2010, **39**, 189-227; (c) J.-C. G. Bünzli and S. V. Eliseeva, *Chem. Sci.*, 2013, **4**, 1939-1949.
3 (a) P. Caravan, J. J. Ellison, T. J. McMurry and R. B. Lauffer, *Chem. Rev.*, 1999, **99**, 2293-2352; (b) P. Caravan, *Chem. Soc. Rev.*, 2006, **35**, 512-523.
4 (a) J. L. Major and T. J. Meade, *Acc. Chem. Res.*, 2009, **42**, 893-903; (b) M. Bottrill, L. Kwok and N. J. Long, *Chem. Soc. Rev.*, 2006, **35**, 557-571; (c) E. J. Werner, A. Datta, C. J. Jocher and K. N. Raymond, *Angew. Chem. Int. Ed.*, 2008, **47**, 8568-8580.
5 (a) S. J. Butler and D. Parker, *Chem. Soc. Rev.*, 2013, **42**, 1652-1666; (b) A. J. Amoroso and S. J. A. Pope, *Chem. Soc. Rev.*, 2015, **44**, 4723-4742.
6 (a) J. Rocha, L. D. Carlos, F. A. A. Paz and D. Ananias, *Chem. Soc. Rev.*, 2011, **40**, 926–940; (b) M. D. Allendorf, C. A. Bauer, R. K. Bhakta and R. J. T. Houk, *Chem. Soc. Rev.*, 2009, **38**, 1330–1352; (c) K. A. White, D. A. Chengelis, K. A. Gogick, J. Stehman, N. L. Rosi and S. Petoud, *J. Am. Chem. Soc.*, 2009, **131**, 18069–18071.
7 (a) D. N. Woodruff, R. E. P. Winpenny, and R. A. Layfield, *Chem. Rev.*, 2013, **113**, 5110–5148; (b) P. Bag, C. K. Rastogi, S. Biswas, S. Sivakumar, V. Mereacre and V. Chandrasekhar, *Dalton Trans.*, 2015, **44**, 4328-4340.
8 N. Sim and D. Parker, *Chem. Soc. Rev.*, 2015, **44**, 2122-2134.
9 (a) M. L. P. Reddy, V. Divya and R. Pavithran, *Dalton Trans.*, 2013, **42**, 15249-15262; (b) S. Biju, D. B. A. Raj, M. L. P. Reddy and B. M. Kulkarni, *Inorg. Chem.*, 2006, **45**, 10651-10660.
10 (a) X. Zhu, W.-K. Wong, W.-Y. Wong and X. Yang, *Eur. J. Inorg. Chem.*, 2011, 4651-4674; (b) J. L. Sessler, T. D. Mody, G. W. Hemmi, V. Lynch, *Inorg. Chem.*, 1993, **32**, 3175–3187.
11 (a) M. C. Hefferin, L. M. Matosziuk and T. J. Meade, *Chem. Rev.*, 2014, **114**, 4496-4539; (b) A. J. Amoroso and S. J. A. Pope, *Chem. Soc. Rev.*, 2015, **44**, 4723-4742.
12 (a) N. J. Farrer, L. Salassa and P. J. Sadler, *Dalton Trans.*, 2009, 10690-10701; (b) M. Ethirajan, Y. Chen, P. Joshi and R. K. Pandey, *Chem. Soc. Rev.*, 2011, **40**, 340-362.

13 (a) J. L. Sessler and R. A. Miller, *Biochem. Pharmacol.*, 2000, **59**, 733-739; (b) J. C. Frias, G. Bobba, M. J. Cann, C. J. Hutchison and D. Parker, *Org. Biomol. Chem*., 2003, **1**, 905-907; (c) G.-J. Chen, X. Qiao, J.-L. Tian, J.-Y. Xu, W. Gu, X. Liu and S.-P. Yan, *Dalton Trans*., 2010, **39**, 10637-10643.
14 (a) A. Hussain, D. Lahiri, M. S. A. Begum, S. Saha, R. Majumdar, R. R. Dighe and A. R. Chakravarty, *Inorg. Chem.*, 2010, **49**, 4036-4045; (b) A. Hussain, S. Gadadhar, T. K. Goswami, A. A. Karande and A. R. Chakravarty, *Dalton Trans*., 2012, **41**, 885-895; (c) A. Hussain, K. Somyajit, B. Banik, S. Banerjee, G. Nagaraju and A. R. Chakravarty, *Dalton Trans*., 2013, **42**, 182-195.
15 (a) A. Chandra, K. Singh, S. Singh, S. Sivakumar and A. K. Patra, *Dalton Trans.*, 2016, **45**, 494-497; (b) S. Dasari and A. K. Patra, *Dalton Trans.*, 2015, **44**, 19844-19855.
16 K. Singh, S. Banerjee and A. K. Patra, *RSC Adv.*, 2015, **5**, 107503-107513.
17 (a) G. Bobba, Y. Bretonnière and J.-C. Frias and D. Parker, *Org. Biomol. Chem*., 2003, **1**, 1870-1872; (b) R. A. Poole, G. Bobba, M. J. Cann, J.-C. Frias, D. Parker and R. D. Peacock, *Org. Biomol. Chem*., 2005, **3**, 1013-1024.
18 K. Toshima, R. Takano, T. Ozawa and S. Matusumura, *Chem. Commun*., 2002, 212-213.
19 (a) J. Shi, Y. Hou, W. Chu, X. Shi, H. Gu, B. Wang and Z. Sun, *Inorg. Chem*., 2013, **52**, 5013−5022; (b) X. Feng, S.-H. Li, L.-Y. Wang, J.-S. Zhao, Z.-Q. Shi and P.-P. Le, *CrystEngComm*, 2012, **14**, 3684–3693.
20 (a) C. Janiak, *J. Chem. Soc., Dalton Trans*., 2000, 3885-3896; (b) K. P. Carter, C. H. F. Zulato and C. L. Cahill, *CrystEngComm*, 2014, **16**, 10189-10202
21 (a) A. Zalkin, D. H. Templeton and D. G. Karraker, *Inorg. Chem*., 1969, **8**, 2680-2684; (b) F. A. Saad, J. C. Knight, B. M. Kariuki and A. J. Amoroso, *Dalton Trans.*, 2013, **42**, 14826-14835.
22 (a) E. C. Long and J. K. Barton, *Acc. Chem. Res*., 1990, **23**, 271-273; (b) A. C. Komor and J. K. Barton, *Chem. Commun.*, 2013, **49**, 3617-3630.
23 (a) T. M. Kelly, A. B. Tossi, D. J. McConnell and T. C. Strekas, *Nucleic Acid Res*., 1985, **13**, 6017-6034; (b) V. A. Bloomfield, D. M. Crothers and I. Tinocoo, Jr., *Physical Chemistry of Nucleic Acids.*, Harper & Row, New York, 1974, pp 432.
24 (a) M. J. Waring, *J. Mol. Biol*., 1965, **13**, 269-282; (b) B. C. Baguley and E.-M. Falkenhaug, *Nucl. Acids. Res.,* 1978, **5**, 161-171.
25 D. L. Boger, B. E. Fink, S. R. Brunnette, W. C. Tse and M. P. Hedrick, *J. Am. Chem. Soc.,* 2001, **123**, 5878-5891.
26 (a) N. S. Quiming, R. B. Vergel, M. G. Nicolas and J. A. Villanueva, *J. Health. Sci.*, 2005, **51**, 8-15; (b) A. Sulkowska, *J. Mol. Struct*., 2002, **616**, 227-232;
27 J. R. Lakowicz, *Principles of Fluorescence Spectroscopy*, 3rd ed., Springer: New York, 2006.
28 M. Y. Li, C. S. Cline, E. B. Koker, H. H. Carmichael, C. F. Chignell and P. Bilski, *Photochem. Photobiol*., 2001, **74**, 760-764.
29 S. M. Klein, G. Cohen and A. I. Cederbaum, *Biochemistry*, 1981, **20**, 6006-6012.
30 J. S. Beckman, T. W. Beckman, J. Chen, P. A. Marshall and B. A. Freeman, *Proc. Natl. Acad. Sci., USA,* 1990, **87**, 1620-1624.
31 (a) A. U. Khan, *J. Phys. Chem*., 1976, **80**, 2219-2228; (b) P. B. Merkel and D. R. Kearns, *J. Am. Chem. Soc.*, 1972, **94**, 1029-1030.
32 D. D. Perrin, W. L. F. Armarego and D. R. Perrin, *Purification of Laboratory Chemicals*, Pergamon Press, Oxford, 1980.
33 (a) J. E. Dickeson and L. A. Summers, *Aus. J. Chem*., 1970, **23**, 1023-1027; (b) J. G. Collins, A. D. Sleeman, J. R. Aldrich-Wright, I. Greguric and T. W. Hambley, *Inorg. Chem*., 1998, **37**, 3133-3141.
34 E. Amouyal, A. Homsi, J.-C. Chamron and J.-P. Sauvage, *J. Chem. Soc., Dalton Trans*., 1990, 1841-1845.
35 *APEX2 v2012.4*, Bruker AXS: Madison, WI, 1999.
36 N. Walker and D. Stuart, *Acta Crystallogr. A.,* 1983, **39**, 158-166.
37 G. M. Sheldrick, *SADABS, Area Detector Absorption Correction*, University of Göttingen, Göttingen, Germany, 2001.
38 G. M. Sheldrick, *SHELX-97, Program for Refinement of Crystal Structures*, University of Göttingen, Göttingen, Germany, 1997.
39 (a) G. M. Sheldrick, *Acta Crystllogr*. 2008, **A64**, 112-122; (b) G. M. Sheldrick, *SHELXTL 6.14*, Bruker, AXS Inc., Madison, WI, 2000.
40 (a) L. J. Farrugia, *WINGX ver. 1.70, An Integrated System of Windows Programs for the Solution, Refinement, and Analysis of Single Crystal X-ray Diffraction Data*, Department of Chemistry, University of Glasgow, 2005; (b) L. J. Farrugia, *J. Appl. Cryst*., 1999, **32**, 837-838.
41 M. N. Burnett and C. K. Johnson, *ORTEP-III, Report ORNL - 6895*; Oak Ridge National Laboratory: Oak Ridge, TN, 1996.
42 J. Marmur, *J. Mol. Biol.,* 1961, **3**, 208-218.
43 M. E. Reichmann, S. A. Rice, C. A. Thomas and P. Doty, *J. Am. Chem. Soc.*, 1954, **76**, 3047-3053.
44 A. Wolfe, G. H. Shimer and T. Meehan, *Biochemistry*, 1987, **26**, 6392-6396.
45 M. Lee, A. L. Rhodes, M. D. Wyatt, S. Forrow and J. Hartley, *Biochemistry*, 1993, **32**, 4237-4245.

**Graphical Abstract for Table of Contents**

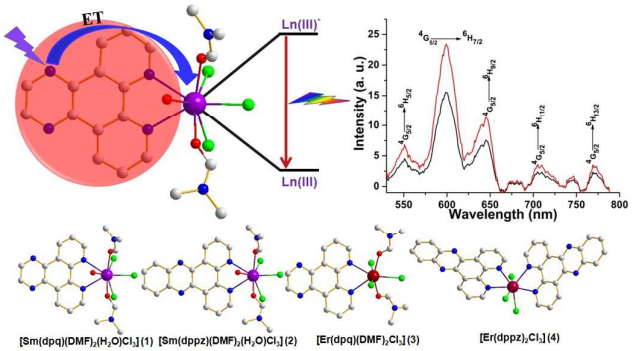


**Graphical Abstract:** A series of Sm(III) and Er(III) complexes of *N*,*N*-donor heterocyclic bases were studied for their crystal structures, luminescent properties, binding with biomolecules and photo-induced DNA damage activity.